X-ray Structure Analyses of Photosynthetic Reaction Center Variants from *Rhodobacter sphaeroides*: Structural Changes Induced by Point Mutations at Position L209 Modulate Electron and Proton Transfer†

Andreas Kuglstatter,‡,§ Ulrich Ermler,‡ Hartmut Michel,‡ Laura Baciou,|| and Günter Fritzsch*,‡

Max-Planck-Institut für Biophysik, H.-Hoffmann-Strasse 7, 60528 Frankfurt/M, Germany, and Centre de Génétique Moléculaire, CNRS, 91198 Gif-sur-Yvette, France

Received July 7, 2000; Revised Manuscript Received December 12, 2000

ABSTRACT: The structures of the reaction center variants Pro L209 → Tyr, Pro L209 → Phe, and Pro L209 → Glu from the photosynthetic purple bacterium *Rhodobacter sphaeroides* have been determined by X-ray crystallography to 2.6−2.8 Å resolution. These variants were constructed to interrupt a chain of tightly bound water molecules that was assumed to facilitate proton transfer from the cytoplasm to the secondary quinone Q_B [Baciou, L., and Michel, H. (1995) *Biochemistry 34*, 7967−7972]. However, the amino acid exchanges Pro L209 → Tyr and Pro L209 → Phe do not interrupt the water chain. Both aromatic side chains are oriented away from this water chain and interact with three surrounding polar side chains (Asp L213, Thr L226, and Glu H173) which are displaced by up to 2.6 Å. The conformational changes induced by the bulky aromatic rings of Tyr L209 and Phe L209 lead to unexpected displacements of Q_B compared to the wild-type protein. In the structure of the Pro L209 → Tyr variant, Q_B is shifted by ∼4 Å and is now located at a position similar to that reported for the wild-type reaction center after illumination [Stowell, M. H. B., et al. (1997) *Science 276*, 812−816]. In the Pro L209 → Phe variant, the electron density map reveals an intermediate Q_B position between the binding sites of the wild-type protein in the dark and the Pro L209 → Tyr protein. In the Pro L209 → Glu reaction center, the carboxylic side chain of Glu L209 is located within the water chain, and the binding site of Q_B remains unchanged compared to the wild-type structure.

The photosynthetic reaction center (RC)[1] of the purple bacterium *Rhodobacter* (*Rb.*) *sphaeroides* is a membrane-spanning pigment−protein complex that converts light energy into chemical free energy. Reliable structural models of the *Rb. sphaeroides* RC have been determined at 2.65 (*1*) and 2.2 Å (*2*) resolution. The RC core consists of two protein subunits, L and M. They possess five transmembrane helices each and bind four bacteriochlorophylls, two bacteriopheophytins, two ubiquinone-10 molecules (UQ_{10}), one non-heme iron (Fe^{2+}), and one carotenoid molecule. Except for the carotenoid, the cofactors and the L and M subunits show a quasi C_2 symmetry with its 2-fold axis perpendicular to the membrane. Starting from a bacteriochlorophyll dimer (D) close to the periplasm, the pigments form two branches, A and B, across the membrane. Each branch consists of a monomeric bacteriochlorophyll, a bacteriopheophytin, and a UQ_{10} molecule (Q_A and Q_B, respectively). Between Q_A and Q_B, the non-heme iron is bound to the protein. With its globular domain exposed to the cytoplasm, a third protein subunit, H, is anchored in the membrane by a single membrane-spanning helix.

In contrast to the high degree of symmetry in its structure, the RC functions in an asymmetric manner (reviewed in ref *3*). After transfer of excitation energy from the light-harvesting complexes to the RC, excitation of D, and charge separation, electron transfer occurs unidirectionally along branch A. An electron is transferred within 200 ps from D to the primary quinone Q_A, and D^+ is reduced within ∼1 μs by a soluble cytochrome c_2 from the periplasm. With a time constant ranging between ∼1 and 100 μs (*4*, *5*), the electron reaches the secondary quinone Q_B. The second photoinduced electron transfer to Q_B yields the quinol form Q_BH_2 after two protons have been taken up from the cytoplasm (*6*). Finally, the ubiquinol is released into the photosynthetic membrane and replaced with an oxidized quinone (*7*).

Analogous to the proton transfer mechanism in other proteins such as the cytochrome b_6f complex (*8*, *9*; for a review, see ref *10*), proton transport from the cytoplasm to the secondary quinone Q_B in the RC presumably occurs via protonatable amino acid side chains and water molecules (*11*). Whereas the involvement of Asp L213 (*10*−*15*), Ser

† This work was in part supported by a PROCOPE grant from the Deutscher Akademischer Austauschdienst e.V. (D/9822825), by the French Ministère des Affaires Etrangères (Grant 99002), by the Max-Planck-Gesellschaft, by the Fonds der Chemischen Industrie, and by the Centre National de la Recherche Scientifique.

* To whom correspondence should be addressed: Max-Planck-Institut für Biophysik, H.-Hoffmann-Str. 7, 60528 Frankfurt/M, Germany. Telephone: (49) 69 967 69 417. Fax: (49) 69 967 69 423. E-mail: Guenter.Fritzsch@mpibp-frankfurt.mpg.de.

‡ Max-Planck-Institut für Biophysik.

§ Present address: MRC Laboratory of Molecular Biology, Hills Road, Cambridge CB2 2HQ, U.K.

|| Centre de Génétique Moléculaire.

[1] Abbreviations: D, primary electron donor, a noncovalently linked bacteriochlorophyll dimer; D_B, B-sided bacteriochlorophyll of D; L209PY, Pro L209 → Tyr mutant; L209PF, Pro L209 → Phe mutant; L209PE, Pro L209 → Glu mutant; Q_B, B-sided ubiquinone; Q_A, A-sided ubiquinone; *Rb.*, *Rhodobacter*; RC, reaction center; *Rp.*, *Rhodopseudomonas*; UQ_{10}, ubiquinone-10.

10.1021/bi001589h CCC: $20.00
Published on Web 03/16/2001

L223 (*13*, *18*), and Glu L212 (*13*, *15*−*21*) in the ultimate proton transfer to Q_B has been demonstrated, the function of other protonatable residues and tightly bound water molecules (*22*, *23*) must be analyzed in more detail. Recently, on the basis of the binding location of Zn^{2+} or Cd^{2+} at the RC surface (*24*), a dominant site of proton entry into the RC has been suggested (*25*). If it is assumed that chains of hydrogen-bonded water molecules observed by X-ray crystallography (*1*) form pathways of proton transfer, Pro L209 has been changed by site-directed mutagenesis to tyrosine, phenylalanine (*26*, *27*), and glutamate (*28*, *29*) in an effort to interrupt a water chain that connects the cytoplasmic side of the RC with Glu L212 (*1*). Since the distance from Pro L209 to Q_B is about 9 Å, the exchange of Pro L209 for aromatic amino acids has been assumed not to affect the electrostatic properties of the Q_B binding site. A structural change in the protein backbone around position L209 was not expected, as Pro L209 is not conserved in the homologous *Rhodopseudomonas* (*Rp*.) *viridis* RC where it is replaced with an alanine.

The effects of the amino acid exchanges at position L209 on the RC function were analyzed using time-resolved spectroscopic measurements. Data obtained for the Pro L209 → Tyr (L209PY) RC variant revealed only small changes in the $Q_A^-Q_B \leftrightarrow Q_AQ_B^-$ equilibrium and in the rate of the first electron transfer compared to the corresponding values of the native protein (*26*), leading to the conclusion that this mutation does not change the structure of the Q_B binding pocket. In the Pro L209 → Phe (L209PF) RC variant, a significant decrease in the rate of the first electron transfer has been observed, possibly indicating changes in the RC structure (*26*). Even more dramatic changes, compared to the wild-type protein, occur in the rates of the proton-coupled second electron transfer and the proton uptake after a second flash (*26*, *27*). Depending on the pH, the second electron transfer is up to 10 times slower in the L209PY RC and up to 15 times slower in the L209PF RC. In the L209PY RC, the rate of proton uptake is similar to the rate of the second electron transfer, whereas in the L209PF RC, these processes are less tightly coupled (*29*). On the other hand, no significant changes in the electron and proton transfer kinetics have been observed in studies on the Pro L209 → Glu (L209PE) variant (*28*, *29*). These results suggested that the introduced aromatic side chains in the L209PY and L209PF RC variants point into the mentioned water chain affecting their proton transfer properties (*26*). To test these assumptions, we have determined the three-dimensional structures of the L209PY, L209PF, and L209PE RC variants by X-ray crystallography, revealing several unexpected structural changes. Functional properties of the mutant RCs are discussed in the context of their three-dimensional structures.

MATERIALS AND METHODS

Protein Purification and Crystallization. The mutant RCs were purified as described previously (*26*) using ultracentrifugation, ammonium sulfate precipitation, and anion-exchange chromatography. The membrane protein was crystallized in detergent micelles by applying the vapor diffusion method with potassium phosphate as the precipitant (*30*, *31*). RC crystals with a maximum size of 3.0 mm × 1.0 mm × 1.0 mm grew within ∼2 weeks. They belong to space group $P3_121$ with the following unit cell dimensions: $a = b = 141.7$ Å and $c = 187.2$ Å.

Data Collection and Model Refinement. X-ray diffraction data at 5 °C were collected in oscillation mode using a 345 mm MAR-Research imaging plate detector at the EMBL Outstation BW7B synchrotron beamline (DORIS ring/DESY, Hamburg, Germany). A single crystal was shifted at least five times along its ϕ-axis during X-ray exposure in the dark so that hardly any radiation decay was observed by visual inspection of the diffracting images. No cutoff for radiation decay was applied. Data reduction and procession were performed using the programs DENZO and SCALEPACK from the software package HKL (*32*). For data refinement, reflections in resolution shells where $I/\sigma(I) \geq 2.0$ and $R_{sym} < 30\%$ have been used. The program package CNS, version 0.3 (*33*), was used for crystallographic model refinement by applying the amplitude-based maximum likelihood target function (*34*). The models were refined using rigid-body refinement of the wild-type model (*1*) against the variant diffraction data, isotropic overall *B*-factor refinement, bulk solvent correction (*35*), simulated annealing (*36*), conjugate gradient minimization (*37*), and individual *B*-factor refinement. To determine without model bias the positions of the introduced L209 side chain, of the ubiquinone cofactor Q_B, and of the surrounding amino acids, simulated annealing omit maps (*42*) were calculated omitting all atoms within 8 Å of residue L209 and Q_B and applying harmonic restraints to atoms within a 2 Å cushion. Geometric parameters of Engh and Huber were used for the protein (*38*), and parameters of Treutlein et al. (*39*), Lancaster and Michel (*40*), and U. Ermler (unpublished data) were used for the cofactors. The models were rebuilt using the graphics program O (*41*), omit maps (*42*) and stereochemical information obtained with the model checking program PROCHECK (*43*). Water molecules were introduced at positions determined by CNS (*33*), if (i) the electron density was more than 1.0 standard deviation above the mean density in the $2|F_{obs}| - |F_{calc}|$ map, (ii) the difference electron density was greater than 3.0 standard deviations over the mean density in the $|F_{obs}| - |F_{calc}|$ map, and (iii) the water positions were consistent with hydrogen bonding requirements. All figures were produced with the graphics program SETOR (*44*).

RESULTS

Data Collection and Model Refinement. The data collection and refinement statistics are listed in Table 1. The high-resolution limits range from 2.6 to 2.8 Å. All data sets are more than 95% complete, and the completeness in the highest-resolution shell is still higher than 95%. The R_{sym} is <6% for all data sets. The variation in the unit cell dimensions among the different RC variant crystals and native RC crystals (*1*) is less than 0.5%.

The free *R*-factors (*45*) of the structures presented here vary between 24.7 and 25.1% (Table 1), using 10% of the diffraction data for cross-validation. The conventional crystallographic *R*-factors converged between 21.7 and 22.1%. The R_{free}-based estimates of the average coordinate error vary between 0.43 and 0.47 Å as derived from a Luzzati plot (*46*) and between 0.25 and 0.39 Å as derived from a σ_A plot (*47*). The average deviations of the mutant RC models from ideal stereochemistry are low. Between 98 and 142 water mol-

Table 1: Data Collection and Refinement Statistics

	L209PY (PDB[a] entry 1F6N)	L209PF (PDB[a] entry 1FNP)	L209PE (PDB[a] entry 1FNQ)
data			
resolution (Å)	2.8	2.6	2.6
no. of unique reflections	52164	64538	65174
multiplicity[b]	1.7 (1.7)	1.6 (1.6)	1.7 (1.6)
completeness (%)[b]	96.0 (95.4)	95.6 (95.0)	96.8 (95.9)
R_{sym} (%)[b,c]	5.9 (27.0)	5.0 (27.2)	5.2 (29.5)
refinement			
R_{free} (%)[d]	25.1	24.8	24.7
R_{cryst} (%)	22.1	21.7	21.7
mean coordinate error			
Luzzati (Å)[e]	0.47	0.46	0.43
σ_A (Å)[f]	0.32	0.25	0.39
rmsd[g]			
bond lengths (Å)	0.0099	0.0090	0.0092
bond angles (deg)	1.3	1.1	1.1
dihedral angles (deg)	24.1	23.8	23.9
improper angles (deg)	2.54	2.47	2.46
no. of water molecules	98	142	137
average *B*-factor (Å^2)			
protein	68.1	59.9	59.6
water	56.9	52.9	52.8
Q_B headgroup	93.3	86.8	95.9

[a] Protein Data Bank (*48*). [b] The corresponding values of the highest-resolution shell are given in parentheses. [c] R_{sym} is the *R*-factor for comparing the intensity of symmetry-related reflections given by the equation $\Sigma|I_n - \langle I_n\rangle|/\Sigma I_n$. [d] Cross-validated *R*-factor (*45*). [e] R_{free}-based estimate of the mean coordinate error from a Luzzati plot (*46*). [f] R_{free}-based estimate of the mean coordinate error from a σ_A plot (*47*). [g] Root-mean-square deviations from ideal geometry values as mentioned in Materials and Methods.

ecules were included in the different models. In comparison, 160 water molecules have been reported for a wild-type RC model at 2.65 Å resolution [*1*; PDB (*48*) entry 1PCR], and 468 water molecules have been modeled into an electron density map of two wild-type RCs at 2.2 Å resolution (*2*; PDB entry 1AIJ).

X-ray Structures of the RC Variants

In the mutant RC structures presented here, L209PY (PDB entry 1F6N), L209PF (1FNP), and L209PE (1FNQ), the protein backbone arrangements are conserved compared to the wild-type RC (*1*; PDB entry 1PCR). Structural changes in the RC variants are observed in the vicinity of the exchanged amino acid residues and around the binding pocket of the secondary quinone Q_B. Additionally, the three RC variants exhibit different Q_B binding positions.

RC Variant L209PY. The introduction of a tyrosine at position L209 induces structural changes of the Asp L213, Glu H173, Thr L226, and Phe L216 side chains as well as of the Q_B position. The water chain reported for the *Rb. sphaeroides* wild-type RC (*1*) is conserved (Figure 1a). The side chain of the introduced Tyr L209 points toward Asp L213 and induces a displacement of the Asp L213 carboxy group of ~1.7 Å compared to its position in the wild-type RC. In addition, the bulky Tyr L209 displaces the Glu H173 and Thr L226 side chains by ~2.6 and ~1.2 Å, respectively (Figure 2c). Despite these shifts of Glu H173 and Thr L226, the hydrogen bond between their side chains appears to be present in this mutant RC. A hydrogen bond not observed in the wild-type RC is formed between the Glu H173 and Arg H177 side chains with a bond length of ~2.6 Å (wild-type distance, ~4.6 Å). The hydroxy group of the introduced Tyr L209 side chain forms no hydrogen bond with its protein environment in contrast to a previous suggestion (*26*). The only potential hydrogen bond partner within a suitable distance of the Tyr L209 hydroxy group is one of the Asp L213 carboxylate oxygens (2.9 Å), but the X−donor−acceptor angle of 89° is unfavorable for hydrogen bond formation. Also, the relative orientation of the Tyr phenol ring plane with respect to the Asp oxygen does not support hydrogen bonding as the Tyr hydroxy hydrogen had to be significantly out-of-plane.

A highly surprising feature of the L209PY variant structure is an ~4 Å shift of Q_B from the distal binding site of the wild-type protein to a position proximal to Fe^{2+} (Figures 1a and 2a). The distance from the hydroxy oxygen of the Tyr L209 side chain to the distal methoxy oxygen ($O2_m$) of Q_B is 5.0 Å. Moreover, the electron density of the Q_B molecule in the L209PY mutant RC is of considerably higher quality compared to the corresponding densities of the L209PF (Figures 1b and 2b) and L209PE (Figure 1c) mutant RCs. However, in the L209PY RC structure, neither a $2|F_{obs}| - |F_{calc}|$ electron density map (Figure 1a) nor a simulated annealing omit map (not shown) allows us to distinguish between the Q_B carbonyl and methoxy groups. Therefore, the orientation of the UQ_{10} ring in the Q_B binding site remains undetermined with regard to a 180° rotation around the quinone phytyl tail. In the L209PY RC structure presented here (Figure 1a), the published Q_B orientation of the charge-separated R26 wild-type structure (*2*; PDB entry 1AIG) has been chosen, where the Q_B headgroup is not only shifted compared to the ground state but also rotated by 180° around an in-plane axis. The electron density around the Q_B phytyl tail of the L209PY mutant RC is shown in Figure 2d. An unambiguous assignment of the quinone tail was possible up to position C_{14}; then two conformations of the tail apparently coexist in the L209PY RC structure (only one conformation is displayed in Figure 2d). The refinement of alternate conformations has not been performed because of the low resolution of 2.8 Å. The electron density also indicates that the Q_B headgroup is tilted by about 30° compared to its orientation in the dark-adapted native RC (Figure 2a). Parallel to this tilt, the side chain of Phe L216 appears to be rotated in the same way and to be moved ~1 Å toward the new position of the quinone ring. No similar reorientation of this phenyl ring has been observed in the structure of the R26 wild-type RC when frozen under illumination (*2*). In our structural model of the L209PY variant, O1 of Q_B, which is bound distally to Fe^{2+}, is within hydrogen bonding distance of the Ser L223 hydroxy oxygen and of the Ile L224 peptide nitrogen, $O2_m$ forms a hydrogen bond to the Gly L225 peptide nitrogen, and the proximal keto (O4) oxygen forms a hydrogen bond to His L190.

RC Variant L209PF. The site of amino acid exchange in the L209PF RC variant is represented in Figure 1b. As in the L209PY RC, the water chain is not interrupted by the introduced residue. Except for Phe L216 and Q_B (Figure 2b,c), the structural changes in the L209PF variant caused by the introduction of the bulky phenyl side chain are very similar to the observed changes in the L209PY RC (Figure 2c). The side chain of Glu H173 might be highly flexible as indicated by the electron density maps. The length of the hydrogen bond between the Glu H173 and Thr L226 side chains appears to be increased from ~2.8 Å in the wild-type structure (*1*) to ~3.2 Å in the mutant protein. In our

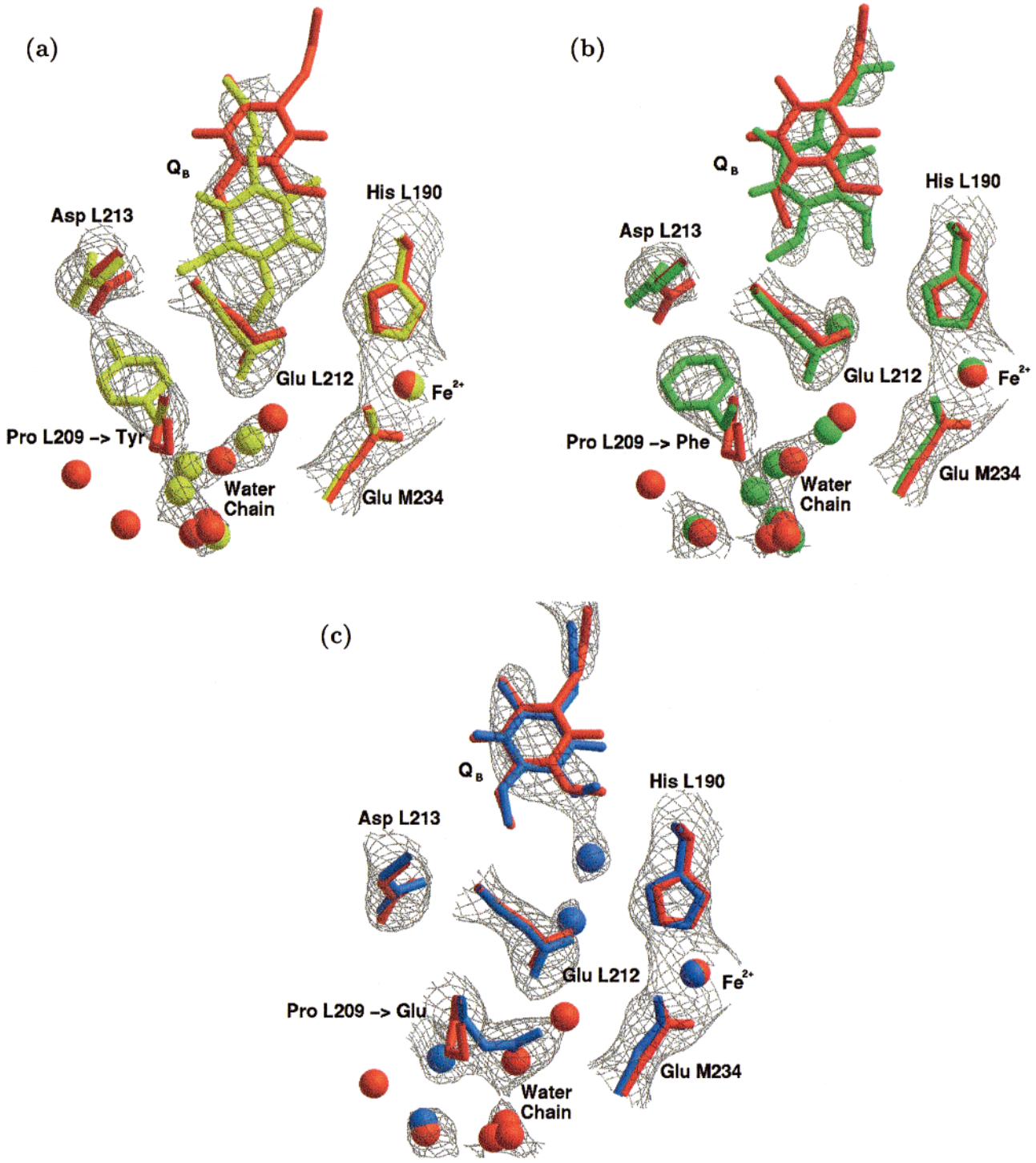

FIGURE 1: $2|F_{obs}| - |F_{calc}|$ electron density maps (1.0σ) at the Q_B binding pocket of the (a) L209PY RC (yellow), (b) L209PF RC (green), and (c) L209PE RC (blue). In all three panels, the wild-type structure (*1*) is drawn in red. The orientation of the Q_B headgroup in L209PY has been modeled on the basis of the light-adapted wild-type RC structure (*2*), and in L209PE, the dark-adapted wild-type RC structure (*1*) was used. The structures have been superimposed by applying a least-squares minimization to the coordinates of all C^{α} atoms within 20 Å of the exchanged amino acid.

L209PF structural model, Glu H173 forms a hydrogen bond to Arg H177. As mentioned above, this hydrogen bond is not observed in the wild-type RC but in the L209PY RC.

The electron density maps shown in Figures 1b and 2b indicate that Q_B in the L209PF variant changes its position compared to the wild-type protein. However, a simulated annealing omit map (data not shown) does not allow an unambiguous identification of the exact Q_B position. The best fit is obtained for an intermediate position of the UQ_{10} molecule between the proximal and the distal binding sites. The mean distance from the Q_B quinol ring to its position in the native RC is 1.7 Å. In this position and orientation (Figure 1b), the distal keto oxygen (O1) of Q_B is within hydrogen bonding distance of the Ile L224 peptide nitrogen and of the Ser L223 hydroxy oxygen. Immediately after, the Q_B headgroup, tracing of the Q_B tail becomes ambiguous. Neither the plane of the quinone ring nor the plane of the Phe L216 phenyl group is rotated significantly compared to

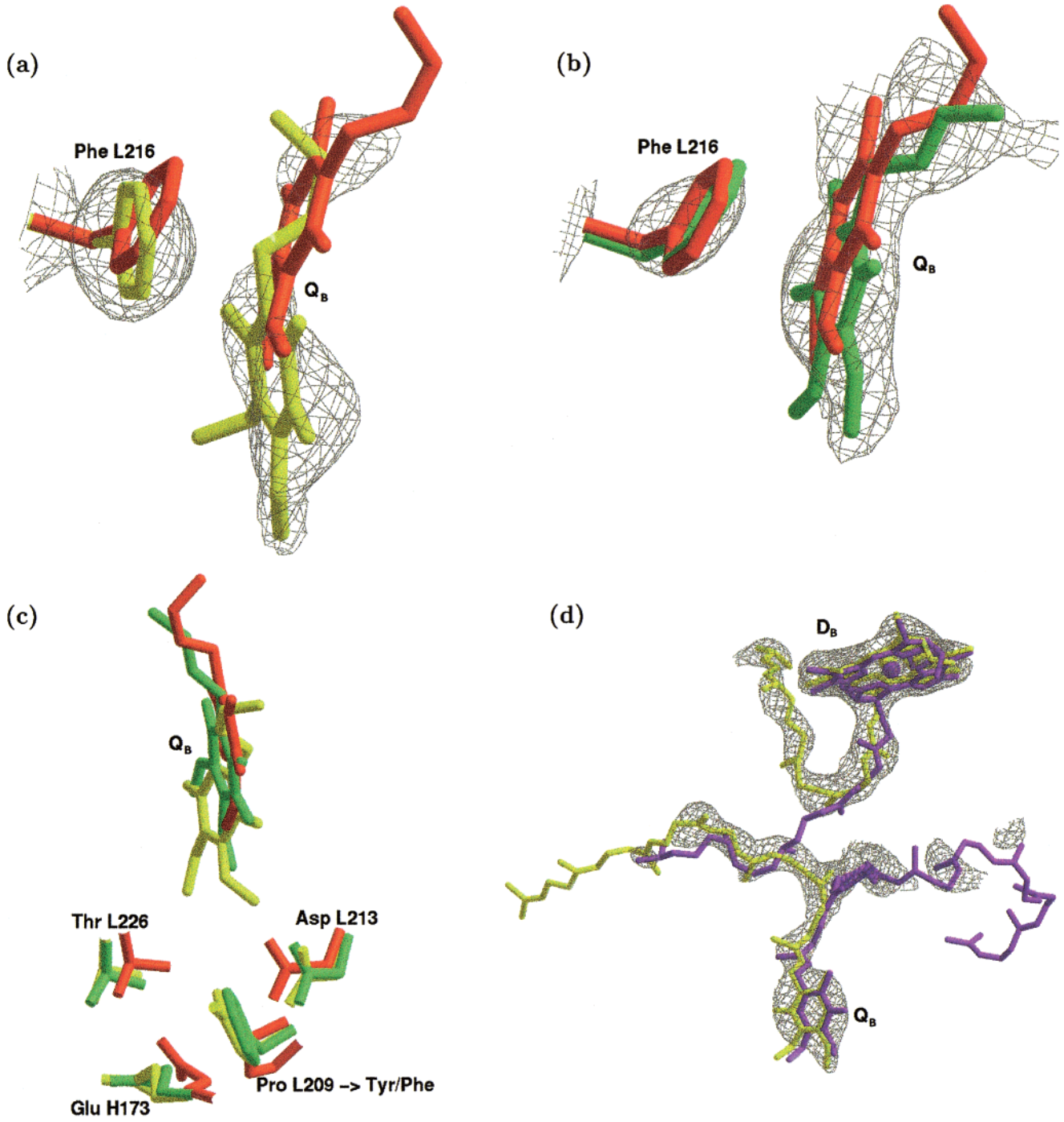

FIGURE 2: Structures of RC variants at the Q_B binding site. $2|F_{obs}| - |F_{calc}|$ simulated annealing omit maps (1.0σ) of the (a) L209PY RC (yellow) and (b) L209PF RC (green). (c) Structural rearrangements in the L209PY RC (yellow) and L209PF RC (green). In panels a−c, the wild-type structure (*1*) is drawn in red. (d) $2|F_{obs}| - |F_{calc}|$ electron density map (1.0σ) of the neutral state of L209FY RC: yellow, L209FY RC (only one conformation of the Q_B tail shown); and lilac, charge-separated state of the R26 wild-type RC (*2*). The structures have been superimposed, and the L209PY Q_B headgroup is modeled as described in the legend of Figure 1.

the wild-type structure (Figure 2b).

RC Variant L209PE. In contrast to the L209PY and L209PF mutant RCs, no significant structural changes are observed in the L209PE structure model (Figure 1c). The introduced Glu L209 side chain replaces two water molecules (nos. 55 and 56 in 1PCR) of the water chain observed in the wild-type RC. $|F_{obs} - F_{calc}|$ electron density difference maps (data not shown) suggest a high mobility of the Glu L209 carboxy group, though this is not supported by a higher-than-average temperature factor. The Glu L209 and Glu L212 side chains are ~2.8 Å apart, and their relative orientations to each other indicate the formation of a hydrogen bond between these residues, suggesting that at least one of these residues is protonated. The side chain of Glu H173 is disordered as indicated by difference electron density maps (data not shown). The electron density of Q_B is not well defined, but it suggests a wild-type-like Q_B position (Figure 1c).

DISCUSSION

Prediction and Reality of the Three Mutant RC Structures. Spectroscopic data led to the hypothesis that the introduced

aromatic residues in RC variants L209PY and L209PF interrupt the water chain mentioned above (*26*) or at least disorganize the hydrogen bonding network involved in proton delivery (*29*). The structural analyses of these two variants at 2.8 and 2.6 Å resolution reveal that both introduced aromatic side chains do not point toward that water chain but toward Asp L213 (Figure 1a,b). Additionally, several unexpected structural changes at the amino acid side chains and of the Q_B position are observed in the L209PY and L209PF structures. For the L209PE mutant RC, no significant alteration of the hydrogen bonding network has been suggested from spectroscopic measurements (*29*). However, the L209PE RC structure at 2.6 Å resolution shows that the introduced Glu L209 side chain replaces two water molecules of the water chain (Figure 1c). In this RC variant, no further structural changes are observed. In the following, the three mutant structures are not discussed in terms of individual water molecules, as the quality and resolution of the diffraction data are not sufficient to determine the positions of water molecules unambiguously.

In the L209PY and L209PF mutant RCs, the location of the introduced bulky aromatic groups between the side chains of Asp L213, Glu H173, and Thr L226 causes very similar conformational changes of these residues of ~1.5 Å compared to the wild-type protein (Figure 2c). Modeling of the structure shows that the predicted positions of Tyr L209 or Phe L209 blocking the water chain would have been possible without structural rearrangements in the protein environment (*26*). Moreover, the structural analysis of the L209PE variant, where the glutamate side chain is oriented into the water chain (Figure 1c), demonstrates that an amino acid exchange at position L209 can lead to the interruption of the water chain. Why Tyr L209 and Phe L209 exhibit side chain orientations different from that of Glu L209 cannot be finally answered from the available structural data. The fact that the shifted side chains of Asp L213, Glu H173, and Thr L226 do not cause further structural changes in their protein environment indicates that the new positions of these residues are not unfavorable, whereas the placement of a glutamate residue between the negatively charged Asp L213 (*13*, *17*) and Glu H173 (*49*) would be electrostatically unfavorable. The lengthening of hydrogen bonds between Glu H173 and Thr L226 in both the L209PY and the L209PF mutant RCs is probably energetically offset by the formation of the hydrogen bond between Glu H173 and Arg H177 that is not present in the native RC.

In the L209PE mutant RC, the introduced glutamate side chain is positioned within the water chain (Figure 1c). A hydrogen bond between Glu L209 and Glu L212 might stabilize the position of the introduced carboxylate within the chain of solvent molecules. The formation of this hydrogen bond requires the protonation of one of the glutamate carboxylates (see the discussion below).

In the neutral state of the wild-type RC, Q_B is predominantly bound at a position distal to Fe^{2+} (*1*, *2*), but partial Q_B occupancy at a position proximal to Fe^{2+} has been observed as well (*2*). For the wild-type RC frozen under illumination, Q_B has been published to be at the proximal position (*2*). Surprising features of the L209PY, L209PF, and L209PE mutant RC structures are the three different locations of Q_B. In contrast to the L209PE RC structure, where the Q_B molecule is found in the distal site (Figure 1c), the quinone in the L209PY structure is observed in the proximal site (Figures 1a and 2a), and in the L209PF RC structure, it is bound at an intermediate position (Figures 1b and 2b). However, the present resolution of the mutant electron density maps does not allow a detailed analysis of changes in the hydrogen bonding patterns at the different Q_B binding sites.

An interesting structural domino effect, not present in the L209PF RC variant, is observed in the L209PY RC variant structure. The introduced Tyr L209 induces indirectly an ~1 Å shift and a 30° rotation of the Phe L216 phenyl ring, which is about 12 Å away from the site of the amino acid exchange. Probably, the Tyr L209 side chain displaces the Asp L213 side chain, and the shift of the Q_B headgroup causes the parallel movement of the adjacent Phe L216 side chain.

The electron density of the L209PY RC variant structure suggests two conformations of the Q_B phytyl chain (only one conformation shown in Figure 2d). In addition, the electron density of the Q_B headgroup is highly symmetrical despite the asymmetrically arranged ubiquinone substituents (Figure 1a), possibly indicating the coexistence of alternative Q_B headgroup conformations. With regard to the observation that in the wild-type RC the movement of Q_B from the distal to the proximal binding position involves a 180° rotation of Q_B (*2*, *40*), the possibility that the putative alternative conformations in the L209PY structure reflect the coexistence of RCs in the states before and after the Q_B rotation cannot be excluded. Additionally, it has to be mentioned that in the L209PY mutant RC the electron densities of D_B and Q_B are clearly separated, whereas the D_B phytyl chain in the light-adapted wild-type structure (*2*) occupies one of the two Q_B tail positions found in the mutant protein (Figure 2d).

Correlation between the Observed Structural Data and the Functional Properties

RC Variant L209PE. In the L209PE RC variant, spectroscopic analysis shows a decrease of the free energy gap between the $Q_A^-Q_B$ and $Q_AQ_B^-$ states, indicating the occurrence of a partial negative charge close to Q_B (*29*). This charge has been suggested to be carried by the Glu L209 carboxy group or, alternatively, by a cluster of highly interacting protonatable residues (Glu L212, Asp L213, Glu H173, and Asp L210), the charge distribution of which may have been changed by the introduction of Glu L209 (*29*). The hydrogen bond between Glu L209 and Glu L212 in the L209PE RC structure supports the latter hypothesis. This hydrogen bond formation requires the protonation of at least one of the glutamate carboxy groups. The protonation state of the introduced Glu L209 in the L209PE protein is not known. In the wild-type RC, it was proposed that Glu L212 possesses an anomalously high pK_a of ~9.5 (*19*, *21*, *50*, *51*), whereas FTIR and kinetic IR data suggest a more ionized Glu L212 (*16*, *52*). Preliminary studies of the pH dependence of the first electron transfer in the L209PE RC variant indicate that Glu L212 might be fully protonated (J. Tandori, P. Sebban, and L. Baciou, unpublished data). Nevertheless, at neutral pH, the L209PE RC variant shows only a small change in the rate of the first electron transfer (*29*). Obviously, the altered charge distribution in the proximity of Q_B, induced by the new hydrogen bond between Glu L212 and the introduced Glu L209, has no significant effect on

the first electron transfer process. In the L209PE RC, the rates of the second proton-coupled electron transfer and of the proton uptake after the second flash are also very similar to the corresponding rates of the native RC (*29*). Apparently, the new hydrogen bond between Glu L212 and the introduced Glu L209 does not influence either the first electron transfer or the second proton transfer to Q_B that involves Glu L212 (*13*). It might be that the hydrogen bonding pattern in the L209PE RC variant mimics that of the wild type (*1*) where the protonated Glu L212 forms two hydrogen bonds with two water molecules (2.7 and 3.2 Å), one of which is replaced with Glu L209 in the mutant RC. If it is assumed that the water chain in the native RC is involved in proton transfer, the introduced Glu L209 carboxy group positioned within the water molecules (Figure 1c) might at least partially take over this function in the L209PE mutant RC.

RC Variants L209PY and L209PF. In the *Rb. sphaeroides* wild-type RC, it was suggested that the anomalously high pK_a of 9.5 assigned to Glu L212 (*19*) results from its interaction with Asp L213 (*13*) and Glu H173 (*20*). In both aromatic RC variants, L209PY and L209PF, the distances between Glu L212 and Asp L213 and between Glu L212 and Glu H173 are increased by about 1.7 and 2.0 Å, respectively, compared to the native protein (Figure 2c). However, the poor effect of the aromatic mutations on the pH dependence of the $Q_A^-Q_B \leftrightarrow Q_AQ_B^-$ equilibrium shows that these structural changes do not result in large pK_a shifts for Glu L212. Apparently, the electrostatic environment of Q_B is not significantly affected by the introduced aromatic residues (*26*), indicating that the local rearrangements within the "acidic cluster" do not result in a significant change in the overall charge distribution. As the minimal distance between Tyr L209 and Q_B is 5.0 Å, electrostatic interactions are possible but probably weak with a neutral tyrosine.

The apparent pK_a value of Asp L213 in the wild-type RC is ~4.5 (*12*). It has been suggested that even small changes in the coordinates of the titrating Asp L213 carboxy group may shift its pK_a value considerably (*53*). In the L209PY and L209PF RC variants, the side chain of Asp L213 is shifted by about 1.5 Å compared to the wild-type structure (*1*). However, preliminary measurements indicate that, in the L209PY RC variant, the pK_a value of Asp L213 is only slightly increased while a much higher upshift of this pK_a is observed in the L209PF RC (J. Tandori, P. Sebban, and L. Baciou, unpublished data). The formation of a hydrogen bond between Asp L213 and Tyr L209 is unlikely with respect to the potential donor−acceptor geometry (see Results). Presumably, the two introduced aromatic L209 side chains affect in a different manner the protonation state of the Asp L213 side chain. This might be due to the different polarities of both side chains.

Recent spectroscopic measurements (*4*, *5*) have shown that the kinetics of the $Q_A^- \rightarrow Q_B$ electron transfer are in fact multiphasic (40−80 and 200−600 μs). According to the proposal in ref *2* and to the mechanistic model for the homologous *Rp. viridis* RC presented in ref *40*, the movement of Q_B from the distal to the proximal position in the *Rb. sphaeroides* wild-type RC is a necessary prerequisite for the first electron transfer ($Q_A^-Q_B \rightarrow Q_AQ_B^-$). In the L209PF mutant RC structure, the existence of an intermediate Q_B position (Figure 1b) not occupied in the wild-type protein may result in a lower level of occupation of the functional proximal Q_B binding site. This might explain the significantly reduced rate of the first electron transfer [>1 ms (*26*)] in this mutant compared to the wild-type kinetics.

It has also been postulated that the ~80 μs electron transfer component measured in wild-type isolated reaction centers might be correlated to a slow rate-limiting step that involves the translation movement of Q_B from the distal to the proximal binding position (*2*, *54*). However, it should be pointed out that, in the L209PY mutant structure, where Q_B binds already in the charge-separated proximal position (Figure 1a), the rate of the first electron transfer is only slightly reduced (~150 μs) (*26*). This observation does not support a direct correlation between the movement of Q_B to reach the proximal position and the measured electron transfer rates.

Similarly, it was proposed recently that Glu H173 is involved in the gating process of the first electron transfer (*55*). These authors have suggested that the mobility of Glu H173 may determine the rate of the gating process, and they correlate a reduction in its mobility (in the presence of Cd^{2+}) to a reduction of the first electron transfer rate. However, in the L209PY mutant structure, the ~2.6 Å-shifted position of the Glu H173 side chain does not affect the first electron transfer rate, suggesting that its position is not the crucial part in determining the proposed gating process. Also, no significant difference between the aromatic mutant RC structures is observed in the temperature factors of the Glu H173 side chains relative to the respective overall protein, in contrast to the different rates in the first electron transfer.

In fact, it was also proposed that proton redistribution via Asp L213 is the rate-limiting step of the first electron transfer (*13*, *15*). Indeed, the first electron transfer rates (*26*) and the estimated pK_a values assigned to Asp L213 were found to be different in the L209PF and L209PY variants (J. Tandori, P. Sebban, and L. Baciou, unpublished data). However, if it is assumed that no hydrogen bond is formed between Asp L213 and Tyr L209 (see Results), very similar hydrogen bond rearrangements are observed in both mutant RCs. This suggests that the same hydrogen bonding pattern can be correlated with different protonation states and electrostatic environments of Asp L213 due to the different effects of the introduced tyrosine or phenylalanine side chains on Asp L213.

Although very similar structural changes are observed in the L209PY and L209PF RC variants, the introduced L209 mutations reduce the rates of the second electron transfer from Q_A to Q_B^- ~2.5- and ~11-fold, respectively (*26*, *29*). We propose that the different rates of the second electron transfer in both aromatic RC variants also result from the different effects of the Tyr L209 and Phe L209 side chains on the protonation states of Asp L213 as discussed above for the first electron transfer. However, in the L209PY and L209PF RC variants, the rates of the proton transfer itself are decreased similarly [~2.5- and ~4-fold, respectively (*26*, *29*)]. Therefore, it was concluded that, in contrast to the wild-type and L209PY RCs, the second electron transfer and proton uptake are not kinetically coupled in the L209PF variant (*29*). In the native RC, Asp L213 has been shown to be involved in the first protonation of Q_B (*13*). In fact, in the L209PY and L209PF RCs, the ~1.4 Å shifts of the Asp L213 side chains compared to the wild-type RC (*1*) cause rearrangements of the hydrogen bonding patterns at the Q_B

binding pockets. This observation indicates that the reduction of the proton transfer rate in the aromatic RCs may result from the new side chain position of Asp L213. Thus, the similar decrease in the rates of proton uptake in the L209PY and L209PF RCs correlates to the similar changes in their structures compared to the wild-type protein. These findings indicate that the electrostatic properties related to the protonation state of Asp L213 influence the proton-coupled second electron transfer more than the proton transfer rate itself which appears to be essentially modulated by the hydrogen bonding pattern at the Q_B binding pocket.

ACKNOWLEDGMENT

We thank Zlata Bojadzijev and Gregor Eichberger for technical assistance, Pierre Sebban for careful reading of the manuscript and helpful discussions, and Victor Lamzin (EMBL outstation, Hamburg) for support at beamline BW7B (DORIS ring/DESY).

REFERENCES

1. Ermler, U., Fritzsch, G., Buchanan, S. K., and Michel, H. (1994) *Structure 2*, 925−936.
2. Stowell, M. H. B., McPhillips, T. M., Rees, D. C., Soltis, S. M., Abresch, E., and Feher, G. (1997) *Science 276*, 812−816.
3. Woodbury, N. W., and Allen, J. P. (1995) in *Anoxygenic Photosynthetic Bacteria* (Blankenship, R. E., Madigan, M. T., and Bauer, C. E., Eds.) pp 527−557, Kluwer Academic Publishers, Dordrecht, The Netherlands.
4. Tiede, D. M., Vásquez, J., Córdova, J., and Marone, P. A. (1996) *Biochemistry 35*, 10763−10775.
5. Li, J., Gilroy, D., Tiede, D. M., and Gunner, M. R. (1998) *Biochemistry 37*, 2818−2829.
6. Okamura, M. Y., Paddock, M. L., Graige, M. S., and Feher G. (2000) *Biochim. Biophys. Acta 1458*, 148−163.
7. McPherson, P. H., Okamura, M. Y., and Feher, G. (1990) *Biochim. Biophys. Acta 1016*, 289−292.
8. Martinez, S. E., Huang, D., Ponomarev, M. V., Cramer, W. A., and Smith, J. L. (1996) *Protein Sci. 5*, 1081−1092.
9. Sainz, G., Carrell, C. J., Ponomarev, M. V., Soriano, G. M., Cramer, W. A., and Smith, J. L. (2000*) Biochemistry 39*, 9164−9173.
10. Meyer, E. (1992) *Protein Sci. 1*, 1543−1562.
11. Beroza, P., Fredkin, D. R., Okamura, M. Y., and Feher, G. (1992) in *The Photosynthetic Bacterial Reaction Center II* (Breton, J., and Verméglio, A., Eds.) pp 363−374, Plenum Press, New York.
12. Takahashi, E., and Wraight, C. A. (1990) *Biochim. Biophys. Acta 1020*, 107−111.
13. Takahashi, E., and Wraight, C. A. (1992) *Biochemistry 31*, 855−866.
14. Rongey, S. H., Paddock, M. L., Feher, G., and Okamura, M. Y. (1993) *Proc. Natl. Acad. Sci. U.S.A. 90*, 1325−1329.
15. Paddock, M. L., Rongey, S. H., McPherson, P. H., Juth, A., Feher, G., and Okamura, M. Y. (1994) *Biochemistry 33*, 734−745.
16. Nabedryk, E., Breton, J., Hienerwadel, R., Fogel, C., Mäntele, W., Paddock, M. L., and Okamura, M. Y. (1995) *Biochemistry 34*, 14722−14732.
17. Maroti, P., Hanson, D. K., Baciou, L., Schiffer, M., and Sebban, P. (1994) *Proc. Natl. Acad. Sci. U.S.A. 91*, 5617−5621.
18. Paddock, M. L., McPherson, P. H., Feher, G., and Okamura, M. Y. (1990) *Proc. Natl. Acad. Sci. U.S.A. 87*, 6803−6807.
19. Paddock, M. L., Rongey, S. H., Feher, G., and Okamura, M. Y. (1989) *Proc. Natl. Acad. Sci. U.S.A. 86*, 6602−6606.
20. Takahashi, E., and Wraight, C. A. (1996) *Proc. Natl. Acad. Sci. U.S.A. 93*, 2640−2645.
21. Miksovska, J., Kalman, L., Schiffer, M., Maroti, P., Sebban, P., and Hanson, D. K. (1997) *Biochemistry 36*, 12216−12226.
22. Fritzsch, G., Kampmann, L., Kapaun, G., and Michel, H. (1998) *Photosynth. Res. 55*, 127−132.
23. Abresch, E. C., Paddock, M. L., Stowell, M. H. B., McPhilips, T. M., Axelrod, H. L., Soltis, S. M., Rees, D. C., Okamura, M. Y., and Feher, G. (1998) *Photosynth. Res. 55*, 119−125.
24. Paddock, M. L., Graige, M. S., Feher, G., and Okamura, M. Y. (1999) *Proc. Natl. Acad. Sci. U.S.A. 96*, 6183−6188.
25. Axelrod, H. L., Abresch, E. C., Paddock, M. L., Okamura, M. Y., and Feher, G. (2000) *Proc. Natl. Acad. Sci. U.S.A. 97*, 1542−1547.
26. Baciou, L., and Michel, H. (1995) *Biochemistry 34*, 7967−7972.
27. Baciou, L., and Michel, H. (1995) in *Photosynthesis: From Light to Biosphere* (Mathis, P., Ed.) Vol. I, pp 683−686, Kluwer Academic Publishers, Dordrecht, The Netherlands.
28. Tandori, J., Sebban, P., Michel, H., and Baciou, L. (1998) in *Photosynthesis: Mechanisms and Effects* (Garab, G., Ed.) Vol. II, pp 865−868, Kluwer Academic Publishers, Dordrecht, The Netherlands.
29. Tandori, J., Sebban, P., Michel, H., and Baciou, L. (1999) *Biochemistry 40*, 13179−13187.
30. Buchanan, S. K., Fritzsch, G., Ermler, U., and Michel, H. (1993) *J. Mol. Biol. 230*, 1311−1314.
31. Fritzsch, G. (1998) *Methods Enzymol. 297*, 57−77.
32. Otwinowski, Z., and Minor, W. (1997) *Methods Enzymol. 276*, 307−326.
33. Brünger, A. T., Adams, P. D., Clore, G. M., DeLano, W. L., Gros, P., Grosse-Kunstleve, R. W., Jiang, J.-S., Kuszewski, J., Nilges, M., Pannu, N. S., Read, R. J., Rice, L. M., Simonson, T., and Warren, G. L. (1998) *Acta Crystallogr. D54*, 905−921.
34. Adams, P. D., Pannu, N. S., Read, R. J., and Brünger, A. T. (1997) *Proc. Natl. Acad. Sci. U.S.A. 94*, 5018−5023.
35. Jiang, J.-S., and Brünger, A. T. (1994) *J. Mol. Biol. 243*, 100−115.
36. Brünger, A. T., Kuriyan, J., and Karplus, M. (1987) *Science 235*, 458−460.
37. Powell, M. J. D. (1977) *Math. Programming 12*, 241−254.
38. Engh, R. A., and Huber, R. (1991) *Acta Crystallogr. A47*, 392−400.
39. Treutlein, H., Schulten, K., Brünger, A. T., Karplus, M., Deisenhofer, J., and Michel, H. (1992) *Proc. Natl. Acad. Sci. U.S.A. 89*, 75−79.
40. Lancaster, C. R. D., and Michel, H. (1997) *Structure 5*, 1339−1359.
41. Jones, T. A., Zou, J.-Y., Cowan, S. W., and Kjeldgaard, M. (1991) *Acta Crystallogr. A47*, 110−119.
42. Hodel, A., Kim, S.-H., and Brünger, A. T. (1992) *Acta Crystallogr. A48*, 851−858.
43. Laskowski, R. A., MacArthur, M. W., Moss, D. S., and Thornton, J. M. (1993) *J. Appl. Crystallogr. 26*, 283−291.
44. Evans, S. V. (1993) *J. Mol. Graphics 11*, 134−138.
45. Brünger, A. T. (1992) *Nature 355*, 472−475.
46. Luzzati, V. (1952) *Acta Crystallogr. 5*, 802−810.
47. Pannu, N. S., and Read, R. J. (1996) *Acta Crystallogr. A52*, 659−668.
48. Abola, E. E., Sussmann, J. L., Prislusky, J., and Manning, N. O. (1997) *Methods Enzymol. 277*, 556−571.
49. Nabedryk, E., Breton, J., Okamura, M. Y., and Paddock, M. L. (1998) *Biochemistry 37*, 14457−14462.
50. Brzezinski, P., Paddock, M. L., Okamura, M. Y., and Feher, G. (1997) *Biochim. Biophys. Acta 1321*, 149−156.
51. Alexov, E. G., and Gunner, M. R. (1999) *Biochemistry 38*, 8253−8270.
52. Hienerwadel, R., Grzybek, S., Fogel, C., Kreutz, W., Okamura, M. Y., Paddock, M. L., Breton, J., Nabedryk, E., and Mäntele, W. (1995) *Biochemistry 34*, 2832−2843.
53. Paddock, M. L., Feher, G., and Okamura, M. Y. (1997) *Biochemistry 36*, 14238−14249.
54. Graige, M. S., Feher, G., and Okamura, M. Y. (1998) *Proc. Natl. Acad. Sci. U.S.A. 95*, 11679−11684.
55. Paddock, M. L., Feher, G., and Okamura, M. Y. (2000) *Proc. Natl. Acad. Sci. U.S.A. 97*, 1548−1553.

BI001589H